

## Article

# Influence of the Magnetization of Thermally Expandable Particles on the Thermal and Debonding Properties of Bonding Joints

Juana Abenojar <sup>1,2,\*</sup> , Sara López de Armentia <sup>2,3</sup>, Juan-Carlos del Real <sup>2,3</sup>  and Miguel-Angel Martínez <sup>1</sup> 

<sup>1</sup> Material Science and Engineering Department, Universidad Carlos III de Madrid, 28911 Leganes, Spain; mamc@ing.uc3m.es

<sup>2</sup> Mechanical Engineering Department, Universidad Pontificia Comillas, 28015 Madrid, Spain; sara.lopez@comillas.edu (S.L.d.A.)

<sup>3</sup> Institute for Research in Technology, Universidad Pontificia Comillas, 28015 Madrid, Spain

\* Correspondence: abenojar@ing.uc3m.es; Tel.: +34-91-624-8374

**Abstract:** This study addresses the challenge of recycling adhesive bonds, as their disassembly is irreversible and damages the substrates. It explores the use of thermally expandable particles (TEPs), which, when heated, expand and weaken the bond. The magnetization of TEPs allows us to control their distribution using a magnetic field. The work aims to obtain magnetized TEPs, study their influence on resin curing, mechanical performance, and durability, test their mobility in graded bonds, and analyze the temperature-induced debonding process. TEPs are characterized using various techniques, including differential scanning calorimetry, nuclear magnetic resonance, and scanning electron microscopy. Additionally, the impact of 25 wt.% TEPs on epoxy resin curing is examined using the Kamal model. Adhesion and disassembly assessments were conducted through tensile shear tests using single-lap-joint specimens, while the bond durability was determined via wedge testing. It was found that magnetization reduces the debonding time, though it decreases shear strength while increasing bond durability. The crack formation energy is higher with magnetic TEPs, and total crack length is lower in long-term wedge tests. Once debonded, the substrates are sanded and reused as raw material.

**Keywords:** thermally expandable particles; magnetic thermally expandable particles; adhesive joints; debonding; durability; wedge test



check for updates

**Citation:** Abenojar, J.; López de Armentia, S.; del Real, J.-C.; Martínez, M.-A. Influence of the Magnetization of Thermally Expandable Particles on the Thermal and Debonding Properties of Bonding Joints. *Inorganics* **2024**, *12*, 129. <https://doi.org/10.3390/inorganics12050129>

Academic Editor: Reshef Tenne

Received: 24 March 2024

Revised: 24 April 2024

Accepted: 26 April 2024

Published: 28 April 2024



**Copyright:** © 2024 by the authors. Licensee MDPI, Basel, Switzerland. This article is an open access article distributed under the terms and conditions of the Creative Commons Attribution (CC BY) license (<https://creativecommons.org/licenses/by/4.0/>).

## 1. Introduction

The automotive industry faces significant challenges related to fuel efficiency requirements, emissions regulations, and environmental concerns, particularly during the end-of-life (EoL) phase. Efforts to enhance vehicle efficiency have led to the use of lightweight materials in structural components, although stricter regulations have resulted in overall weight increases [1]. European Union regulations aiming for emission reduction and improved energy efficiency by 2030 have promoted the use of lightweight and composite materials in passenger vehicles. This has introduced the challenge of finding appropriate joining techniques, especially between dissimilar materials such as metals and non-metals or composites [2].

Recycling at the end of the vehicle's life has become more complex due to the variety of materials used and difficulties in separation [3]. Adhesive bonding techniques and composite materials further complicate the recycling process. End of Life Vehicles (ELVs) constitute a significant waste stream, drawing attention from scholars and industrial stakeholders. Despite extensive research, knowledge gaps remain regarding future ELV volumes and trends. D'Adamo et al. [4] assessed the potential relationship between European ELV flows (including generated and recycled volumes) and two pivotal variables—Gross Domestic

Product (GDP) and population—employing a linear regression model. Their findings revealed that a USD 1000 increase in GDP corresponds to an additional +350 g of recycled ELVs and +10.7 kg of recycled ELVs per capita. Projections for 2030 estimate the amounts of generated and recycled ELVs at 9.3 and 8.3 million tons, respectively [5]. Managers, as indicated by a Likert scale, prioritize economic considerations and the integration of Circular Economy principles with technological advancements [6]. Additionally, by 2030, the trend toward light-weight passenger vehicles will result in over 26.3 million retired vehicles, yielding 19.1 million tons of recyclable steel and 6.2 million tons of plastics [7]. The theoretical economic value of these resources is projected to reach USD 14.4 billion, highlighting the need for vehicle producers to make the transition towards manufacturing models that embrace ELV recycling opportunities. Scenario analysis underscores the necessity for advancements in recycling and reuse technologies for plastics and rubbers to accommodate the growing trend towards lighter-weight vehicles [8].

The choice of lightweight materials for fuel savings and collision performance has led to the use of new multi-materials and composite structures [9]. However, the increased use of lightweight materials has not necessarily led to a reduction in greenhouse gas emissions due to vehicle weight increases from design modifications. Moreover, joining different materials can cause galvanic corrosion, requiring additional design efforts to mitigate issues [10].

In summary, the automotive industry continuously evolves to meet environmental and efficiency standards, leading to the adoption of new materials and joining techniques, as well as challenges in recycling and managing materials at the end of the vehicle's life.

Adhesive bonding is widely used in the industry due to its specific capabilities and advantages, particularly in combining challenging materials such as metals with composites and polymers [11–14]. Adhesives like epoxy, polyurethane, and acrylics offer high structural strength and load-bearing capacities. However, handling them can be tricky, as they require special surface treatments [15–17] and extended curing times [18,19]. Nevertheless, adhesives offer benefits such as weight reduction, improved stress distribution, and increased corrosion resistance [15,20]. In the automotive industry, adhesives are employed for various purposes, from enhancing structural rigidity to sealing components [21]. Moreover, foaming additives are used to enhance adhesion and corrosion protection in bodywork applications [22,23]. Ongoing research in the scientific community seeks to optimize adhesive bonding for diverse applications. Despite this, adhesive joints present two very important challenges in terms of recycling [24] and stress distribution [25–28] along the adhesive joint, particularly in joints with rigid adhesives such as epoxy resins.

Recycling bonding joints is not easy since it is an irreversible process and adhesive joints cannot be disassembled without damaging the substrates. The development of a reversible adhesive, capable of “debonding on-command” has sparked interest in both research and industrial circles. These adhesives require strong adhesive properties, easy reversibility within practical timeframes (preferably seconds to minutes), low toxicity, and compatibility with bonded substrates. Ideally, the cost should be comparable to current adhesives and it should be sourced sustainably [29].

At the industrial level, reactive adhesives, particularly epoxies and polyurethanes, are more suitable for structural applications. They can be utilized across various materials such as metals, ceramics, polymers, and composite materials like CFRP (carbon fiber reinforcement polymer) or GFRP (glass fibers reinforcement polymer) [30]. These adhesive families can be adapted for reversibility due to their low shrinkage, the absence of organic volatile emissions during curing, versatility in terms of viscosity, and a wide range of working temperatures. Moreover, they can be derived from natural oils, making them bio-based compounds and eliminating hazardous compounds [31,32]. However, these adhesives are thermosetting, hence they are infusible and insoluble. Studies on adaptable covalent networks often focus on vitrimers which have a dynamic covalent bond [33–35] that responds to stimuli such as pH, light, or heat, resulting in reversible covalent bonds. Consequently, they are suitable for incorporation into thermosetting materials to obtain

reversible adhesives [36]. However, they are still under investigation and are not yet available on the market.

On the other hand, while a reversible adhesive would be highly desirable for its ability to facilitate repeated bonding and debonding, it would also be intriguing to explore an adhesive that debonds easily. Some researchers have investigated the addition of thermal expansion particles (TEPs) or thermal-expansion materials (TEMs). These particles can be incorporated into the adhesive and are activated within a low temperature range, ranging for example from 90 to 130 °C, facilitating debonding while accommodating various material types [29,37].

The influence of incorporating TEPs into two-component adhesives has been examined for both epoxies and polyurethanes [38–40], as well as different adherents [41]. The impact of TEPs varies depending on the rigidity of the adhesive; the more rigid the adhesive, the higher its cross-linking density, consequently reducing the free volume and restricting reticular mobility. Thus, the expansion temperature of the TEPs is contingent upon both the adhesive's rigidity and the quantity of TEPs introduced. Additionally, environmental factors such as humidity and temperature were investigated [42–44], along with absorption and desorption processes [45]. Changes leading to increase ductility are more contingent on the type of adhesive used rather than on the addition of particles.

Other techniques for debonding joints were studied, including the work of Ciardiello et al. [46] who investigated the addition of iron or iron oxide particles to modify a hot-melt adhesive, thereby imparting a reversible behavior with 5 wt.% of iron and iron oxide. Iron oxide particles with a size of 50 nm yielded the most favorable outcomes on epoxy/glass fiber adherents.

In this line of magnetic particles, it is intriguing to create a customized particle distribution by magnetizing the particles and manipulating them through the application of a magnetic field. This facilitates a uniform distribution of loads across the adhesive joint, a concept known as graded joints, such as the joints with magnetic cork particles [47] or magnetite particles [48]. This would help mitigate another issue in adhesive joints, which can also be achieved by using different cures along the joint [49,50], different adhesives in the same joint [51,52], or different concentration of particles [53,54].

The incorporation of magnetic TEPs presents a novel approach for addressing the drawbacks observed in adhesive joints. The objectives of this study include obtaining magnetic particles from TEPs [55], evaluating the properties of adhesives with and without magnetic TEPs, assessing particle mobility, investigating adhesive bond strength, examining the debonding process, and studying joint durability and adherend recovery.

This study introduces a novel approach by incorporating magnetic TEPs, offering potential applications in facilitating adhesive joint recycling and creating graduated joints. Once the substrates are debonded, they can be sanded or shot blasted and reused as a raw material.

## 2. Results

### 2.1. Characterization of Thermally Expandable Particles

Figure 1 illustrates the thermograms corresponding to the original TEPs, those treated with low pressure plasma (LPP), and magnetic TEPs. While parameters are typically obtained during the second scan, in this case, they were calculated during the first scan due to the expansion of the TEPs with temperature. The melting temperature (Table 1) appears to be consistent across the types of TEPs studied. However, the melting enthalpies decrease with the treatment conducted compared to the original TEP, showing reductions of 9% and 52% for LPP-treated and magnetic TEPs, respectively. The expansion of the TEPs occurred approximately between 120 °C and 125 °C. Although  $T_g$  might be present in this range, confirming its location is challenging due to the overlap of the transitions. Furthermore, magnetic TEPs exhibit a water evaporation peak at 45 °C, which may be absorbed or retained during the magnetization process.

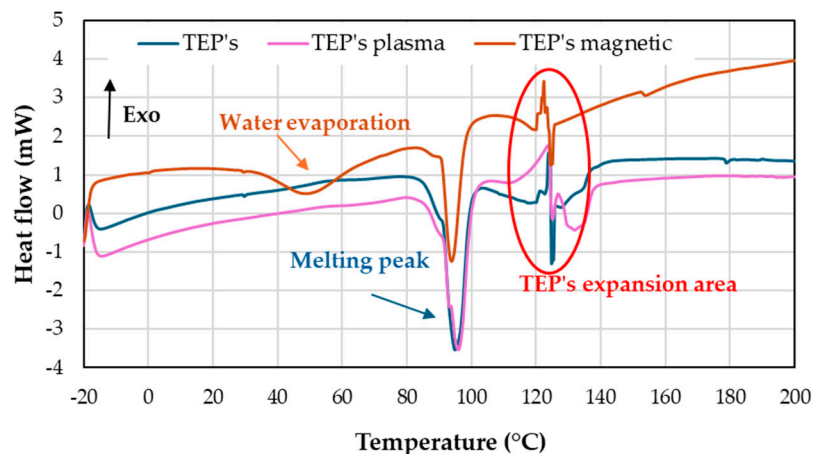
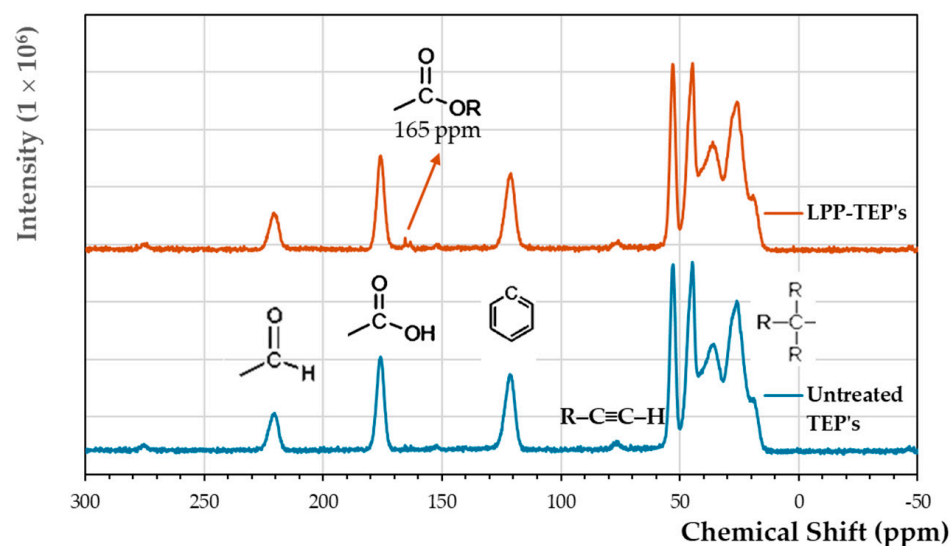


**Figure 1.** Characterization of as-received, LPP-treated, and magnetic TEPs by DSC.

**Table 1.** Thermal properties of TEPs.

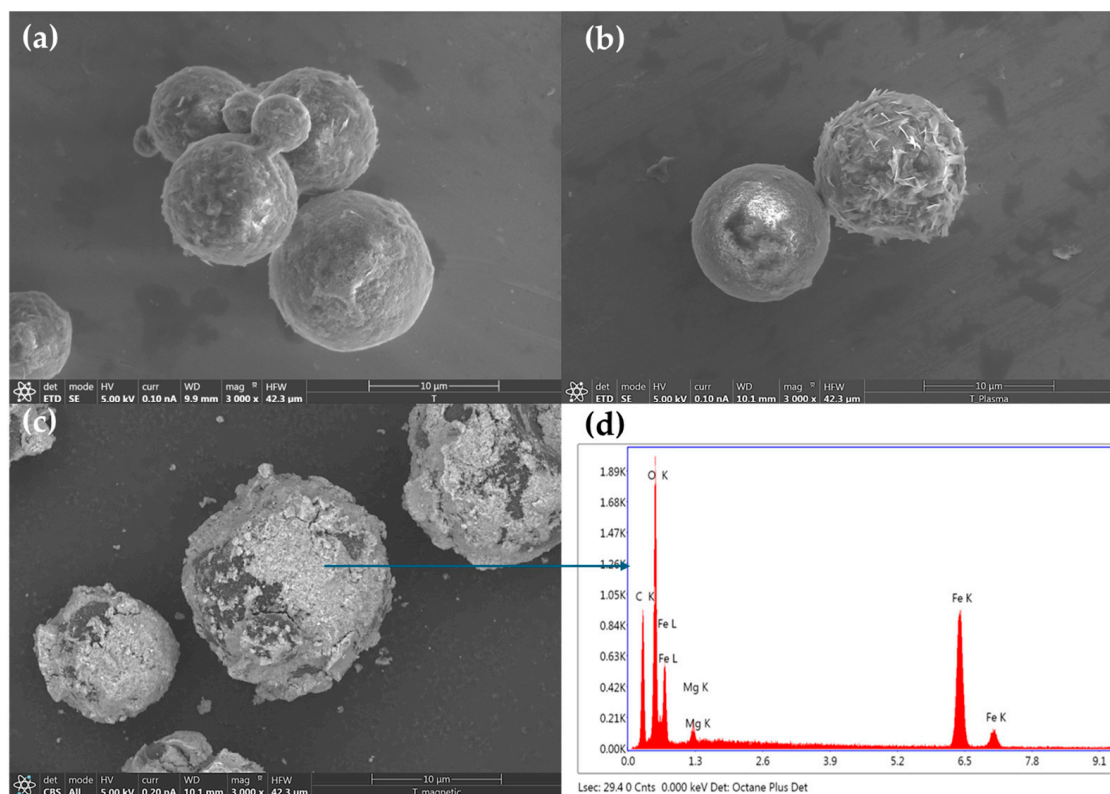
Specimens	$\Delta H_{\text{water}}$ ( $\text{J g}^{-1}$ )	$T_m$ ( $^{\circ}\text{C}$ )	$\Delta H_m$ ( $\text{J g}^{-1}$ )	$T_{\text{TEPs expansion}}$ ( $^{\circ}\text{C}$ )
TEPs		95	−64	120–125
LPP TEPs		96	−58	120–125
Magnetic TEPs	−16	94	−31	120–125

The NMR spectra from 20 ppm to 54 ppm (Figure 2) show five peaks corresponding to the tertiary alkyl; at 78 ppm, a small peak associated with an alkyne group is observed. The aromatic ring of the phenyl radical is found at 123 ppm. A doublet at 165 ppm appears or increases due to the plasma effect, which may correspond to an ester or an amide. The carboxyl group appears at 177 ppm and the aldehyde or ketone group at 221 ppm.



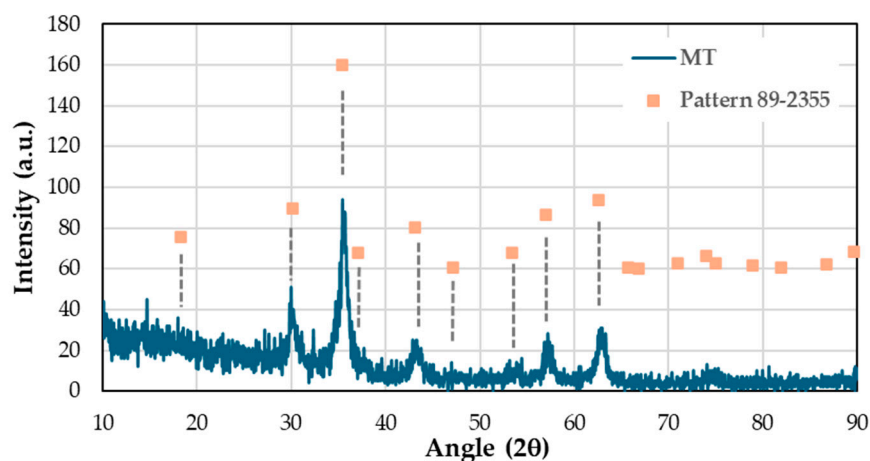
**Figure 2.** Carbon-13 NMR spectra, obtained by MAS, for TEPs before and after LPP treatment.

Figure 3 shows the TEP microcapsules in the three states, as-received (Figure 3a), LPP-treated (Figure 3b), and magnetic (Figure 3c). Figure 3d corresponds to the EDAX performed on the magnetic particles in the coated areas to check for the presence of iron. Oxygen, carbon, magnesium, magnesium, and iron were found in the EDAX.



**Figure 3.** Micrographs of (a) as-received TEPs, (b) LPP-treated TEPs, (c) magnetic TEPs, and (d) EDAX spectrum on magnetic particles.

The presence of magnetite on the TEP particles was confirmed through XRD analysis. The diffractogram peaks observed indicate the presence of iron oxides (Figure 4). Specifically, peaks corresponding to  $\text{Fe}_3\text{O}_4$  were identified at  $2\theta$  values of  $30.1^\circ$ ,  $35^\circ$ ,  $43^\circ$ ,  $53^\circ$ ,  $56.9^\circ$ , and  $62.5^\circ$ , which can be attributed to planes (220), (311), (400), (422), (511), and (440), respectively [56].



**Figure 4.** XRD of magnetic TEPs and magnetite (filled square) patterns.

## 2.2. Influence of the Addition of TEPs on Adhesive Curing Kinetics

The adhesive used was Araldite<sup>®</sup> LY 1564+Aradur<sup>®</sup> 5003 (hardener). To manufacture the composite materials, TEPs and magnetic TEPs were added at 25 wt.%, with a manual mixing to avoid damaging the TEPs. An isothermal scan followed by a dynamic scan were carried out to determine the total enthalpy reaction ( $\Delta H_{\text{Total}} = \Delta H_{\text{isothermal}} + \Delta H_{\text{dynamic}}$ ).

Differential scanning calorimetry (DSC) isothermal tests at 40 °C, 60 °C, and 80 °C were performed to study the kinetic curing reaction.

Reactions between the OH groups of the TEPs and the amine of the hardener may occur since it is easier than the reaction between amine and oxirane rings and it release less energy, as shown by the measurements of  $\Delta H_{\text{Total}}$ . These values were  $292 \pm 4 \text{ J g}^{-1}$  and  $167 \pm 2 \text{ J g}^{-1}$  for +25T and +25MT, respectively, while for pure resin,  $\Delta H_{\text{Total}}$  was  $363 \pm 4 \text{ J g}^{-1}$ . This agrees with a greater amount of OH groups.

These OH groups are also enhanced by the plasma treatment conducted on the TEPs to improve their adhesion to the resin and facilitate the adsorption of magnetite onto the surface during the magnetization process, which is not viable without the pretreatment.

From the isothermal thermograms, the degree of conversion ( $\alpha$ ) was obtained, by Equation (1).

$$\alpha = \frac{\Delta H_t}{\Delta H_{\text{Total}}} \quad (1)$$

where  $\Delta H_t$  and  $\Delta H_{\text{Total}}$  are the exothermic enthalpy during the curing time (120 min) and the exothermic enthalpy for total curing, respectively. Figure 5 shows the three curves at the different temperatures.

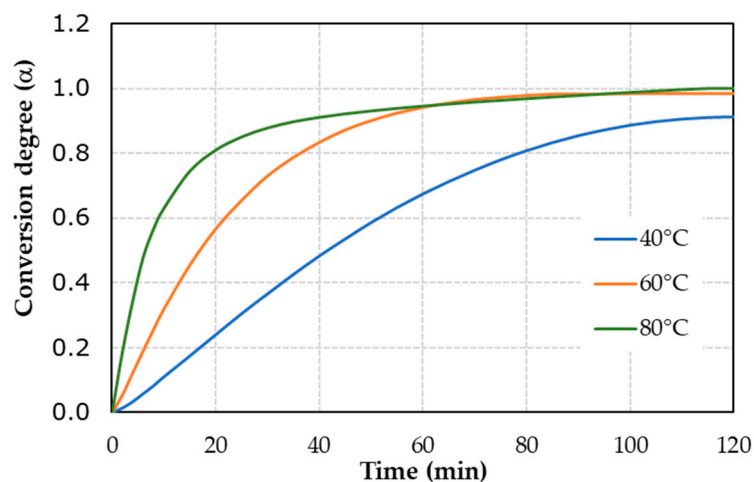


**Figure 5.** Conversion degree at 40 °C, 60 °C, and 80 °C for 1564 + 5003 + 25TEPs.

The derivative of  $\alpha$  with respect to time gives a constant ( $k$ ) and a function of  $\alpha$  (Equation (2)). The calculation of the kinetic parameters was carried out using Kamal's equation (Equation (3)).

$$\frac{\partial \alpha}{\partial t} = kf(\alpha) \quad (2)$$

$$\frac{\partial \alpha}{\partial t} = (k_1 + k_2 \alpha^m)(1 - \alpha)^n \quad (3)$$

Kamal's equation integrates the two curing mechanisms that occur in epoxy resins. Initially, the reaction proceeds slowly, reaching 15% to 20% conversion, following an  $n$ -order mechanism. During this stage, the amino group initiates the opening of the oxirane ring, forming OH groups. These OH groups catalyze the reaction, representing the auto-catalytic mechanism from 20% conversion to approximately 80% conversion, facilitating the crosslinking of the resin. Towards the end of the reaction, the  $n$ -order mechanism re-emerges as fewer groups remain to complete the reaction, resulting in a slower rate of reaction.

In Equation (3),  $k_1$  and  $n$  correspond to the  $n$ -order reaction, where  $k_1$  is the constant and  $n$  is the order of the reaction. Meanwhile,  $k_2$  and  $m$  represent the constant and order of the auto-catalytic reaction. When  $d\alpha/dt$  is plotted versus  $\alpha$ , the curve can be analyzed using a calculation software, such as Origin 6.0, to obtain the kinetic parameters (Figure 6).

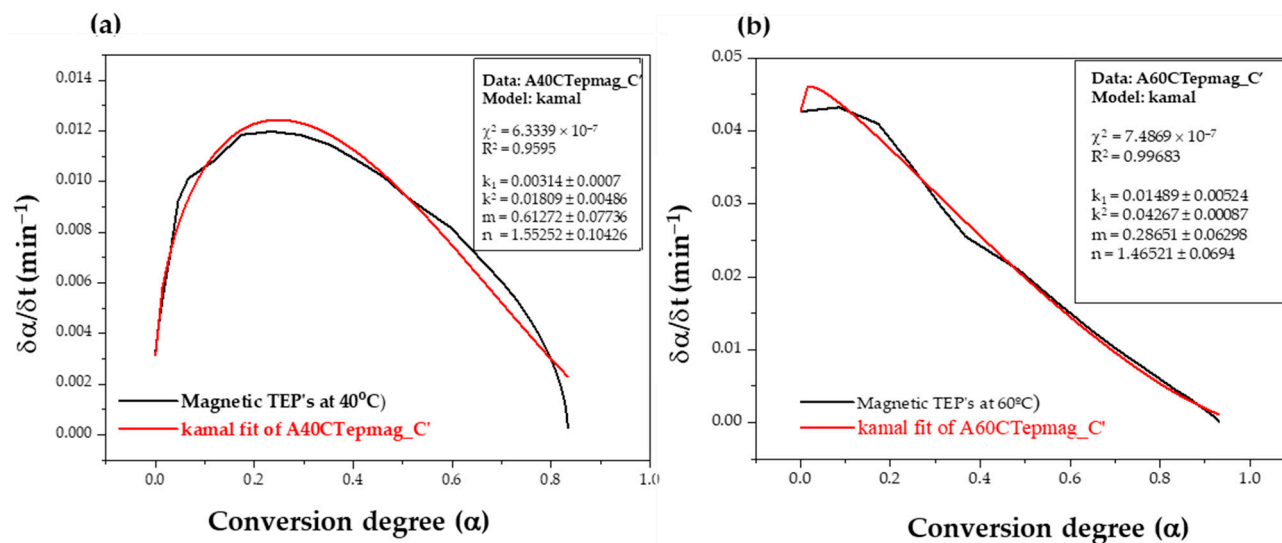


**Figure 6.** Kamal fitting curve (Equation (3)) for the composite with 25% magnetic TEPs (a) at 40 °C and (b) 60 °C.

Figure 6 shows the differences in the curves obtained for 40 °C (Figure 6a) and 60 °C (Figure 6b). The shape of the curve in Figure 6a indicates the presence of both auto-catalytic and n-order mechanisms, and at the end of the curve, the lack of fit suggests that there may be a diffusion mechanism. However, Figure 6b fits to an n-order mechanism. Therefore, it could be concluded that, at 80 °C, the n-order mechanism remains predominant.

The degree of conversion at 120 min is presented in Table 2 for each temperature, along with the corresponding kinetic parameters obtained, as illustrated in Figure 5. The adhesive (1564 + 5003) cured to 74%, 96%, and 100% at 40 °C, 60 °C, and 80 °C, respectively. When 25% of TEPs (+25T) was added, the degree of conversion changed to 91%, 98%, and 100%, respectively. For the 25% magnetic TEPs (+25MT), the conversion rates were 83%, 93%, and 100%. Therefore, only at 40 °C did the +25T accelerate the curing process.

**Table 2.** Kinetic parameters for pure resin and composite.

Samples	Temperature (°C)	$\alpha_{\max}$ 120 min	Kinetic Parameters				$R^2$
			$k_1$	$k_2$	$m$	$n$	
1564 + 5003	40	0.74	0.007	0.004	0.086	0.894	0.98
	60	0.96	0.029	0.018	0.130	1.110	0.97
	80	1	0.125	0.068	0.467	1.441	1.00
+25T	40	0.91	0.005	0.023	0.498	1.074	0.97
	60	0.98	0.016	0.033	0.521	1.084	1.00
	80	1	0.110	0.209	1.007	1.094	1.00
+25MT	40	0.83	0.003	0.018	0.613	1.553	0.96
	60	0.93	0.015	0.043	0.287	1.465	1.00
	80	1	0.074	0.145	0.875	1.500	0.99

In the case of pure resin, the constant  $k_2$  has a lower value than  $k_1$ , which means that the slowest reaction is the auto-catalytic (Table 2). However, if +25T is added, the auto-catalytic process accelerates, while the n-order mechanism slows down the reaction. For +25MT the n-order reaction is also slower than auto-catalytic reaction. The total reaction order ( $m + n$ ) increases with the addition of TEPs. Moreover, it is higher for +25MT than for +25T. The fits of the curves (Figure 6) to the Kamal's equation (Equation (3)) present  $R^2$  values above 0.96.

Since two mechanisms were considered, two rate constants were determined. In the stages where the chemical kinetics governed the reaction, the rate constants show an Arrhenius-type dependence on temperature, as shown in Equation (4). Where  $R$  is the gas constant,  $T$  is the temperature in Kelvin degree, and  $E_a$  is the activation energy of the curing reaction.  $A$  represents the frequency factor or attempt frequency of the reaction, related to the frequency of collisions that lead to a reaction per unit of time.

$$k = Ae^{\frac{-E_a}{RT}} \quad (4)$$

Taking natural logarithms in Equation (4), the Equation (5) is obtained. The plot of Equation (5) gives a straight line (Figure 7), from the slope of which  $E_a$  can be calculated, and the frequency factor  $A$  is obtained from the ordinate at the origin.

$$\text{Ln}k = \text{Ln}A - \frac{E_a}{RT} \quad (5)$$

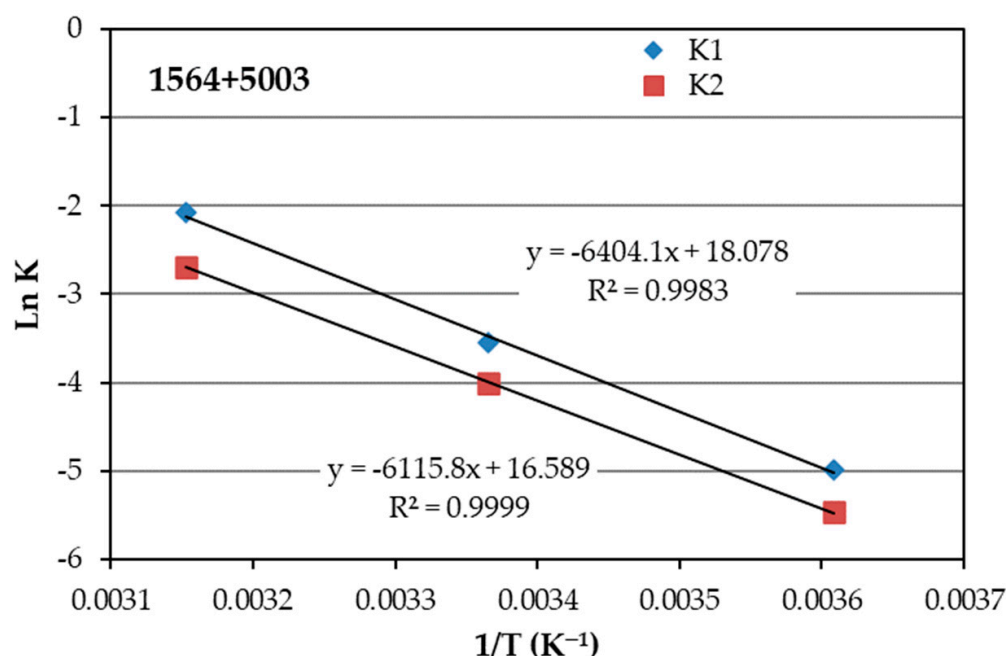


Figure 7. Plot of Equation (5) for composite +25MT.

The  $E_a$  values for the n-order and autocatalytic mechanism have been calculated from Equation (5) (Table 3). The autocatalytic reaction is the slowest for the resin (Table 2), while a slightly higher  $E_a$  is required for the n-order process (Table 3). It is also worth mentioning that, within the pure resin, both the autocatalytic process and the n-order reaction share comparable  $E_a$  values; however, in the composites, the  $E_a$  of the two reactions present more marked differences. In the case of the TEP adhesives, the n-order process is the slowest (Table 2) and the  $E_a$  is the highest (Table 3).

Table 3. Activation energy  $E_a$  by  $k_1$  and  $k_2$ , using Equation (5).

Resin/Composites	$k_1$ $E_a$ (kJ mol <sup>-1</sup> )	$k_2$ $E_a$ (kJ mol <sup>-1</sup> )
1564 + 5003	53	51
+25T	56	40
+25MT	58	38

After 8 days of curing at room temperature, the resin exhibited a  $T_g$  of 78 °C. However, a curing peak emerged as the temperature rose thereafter. Following the supplier's datasheet, a post-curing of 4 h at 60 °C was required. The resulting  $T_g$  was 107 °C in the initial scan, accompanied by a minor relaxation enthalpy peak. In a subsequent scan, the  $T_g$  rose to 117 °C [19]. This temperature closely aligns with the expansion temperature of TEPs. Thermograms conducted for adhesives containing TEPs cannot be analyzed due to the close proximity of the two temperatures. Consequently, no distinct  $T_g$  is detected at temperatures lower than that of the initial sweep of the pure resin.

### 2.3. Examine the Debonding Process Occurring Due to Temperature

The strength of the adhesives' joints was tested through tensile shear tests conducted on single-lap-joint (SLJ) specimens. All tests were carried out with post-cured samples. Figure 8a illustrates one of the five tests conducted for each sample, exhibiting a representative value, close to the average. Figure 8b displays the average of all tests for each adhesive. The shear strength experienced a 27% increase for the +25T adhesive, while it decreased by 10% for the +25MT compared to the pure resin. Moreover, the modulus decreased by 15% for +25T and +25MT.

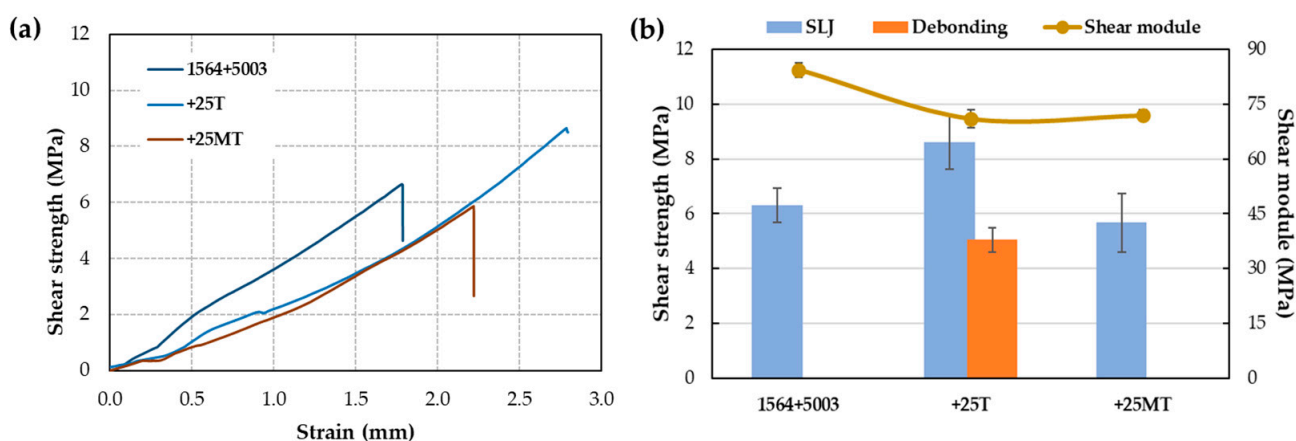


**Figure 8.** SLJ Shear strength tests: (a) representative tests of pure resin and composites, and (b) shear strength, shear module, and strength.

Five other TEP adhesive specimens were subjected to heating up to disassembly or debonding. After warm-up at 115–130 °C for 30 min, samples with +25T had a remaining strength (around 55%), so the specimens did not break completely (Figure 8b). However, the +25MT specimens broke at a lower temperature and after less time, close to 110 °C for 10 min.

The samples are placed into a preheated oven set to 90 °C. In the adhesive bonds with +25MT, swelling of the bonding was immediately apparent (Figure 9a), even at the edges, where the expulsion of some particles was observable (Figure 9b). Figure 9b,c capture the same phenomenon, with one taken using a thermal camera and the other with a digital camera, respectively. The joint spontaneously opened, as depicted in Figure 9d. The joints with +25T also swelled, but did not break; they should be left for a much longer period for debonding.

The SEM micrographs show the fracture of the two joints. The fracture of the +25T joint (Figure 10a) shows flatter areas where the TEPs have not swelled and regions with burst TEPs. However, the appearance of the +25MT fracture (Figure 10b) is notably different, as it does not resemble a shear fracture but rather results from internal forces acting in all directions.

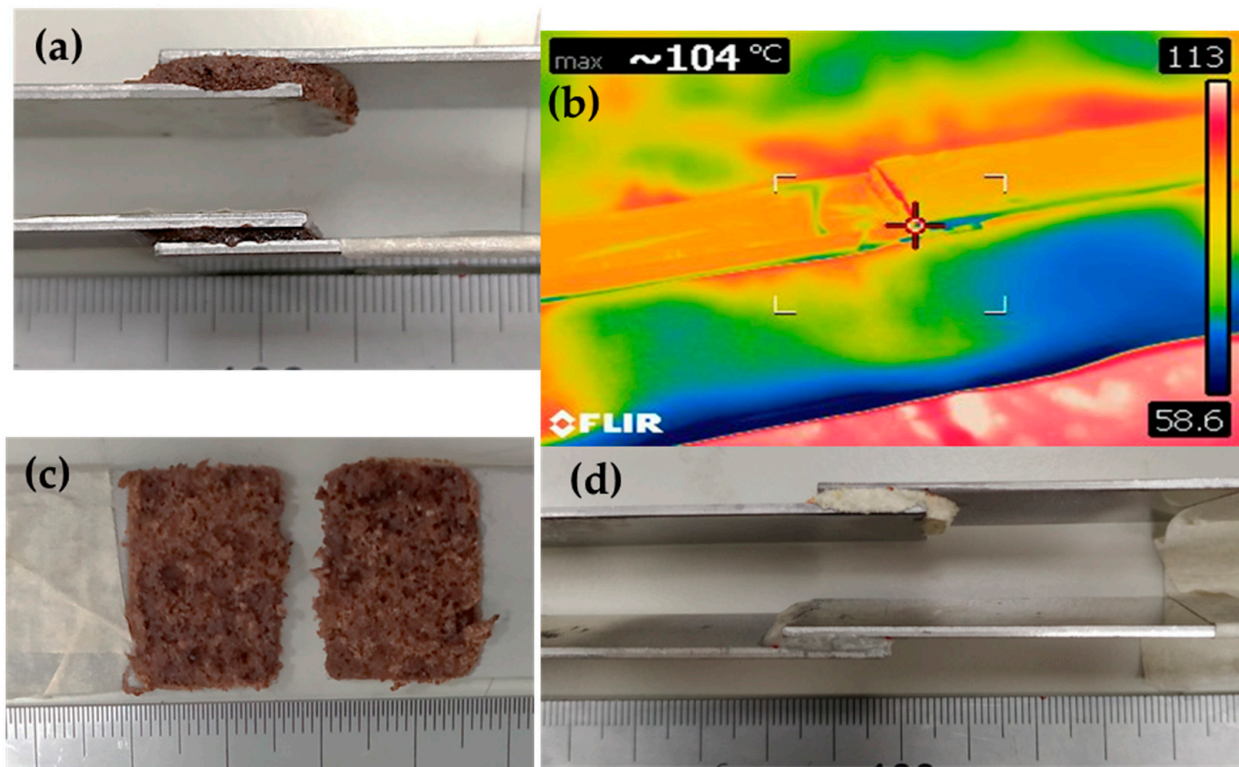


**Figure 9.** Macrographs and thermal images of +25MT debonding. (a) Below: the adhesive joint before heating, and above: the adhesive joint beginning to swell during heating. (b) Infrared image during heating up to 104 °C, showing the onset of swelling. (c) After complete breakage. (d) Macrographic image of +25T: maximum swelling.

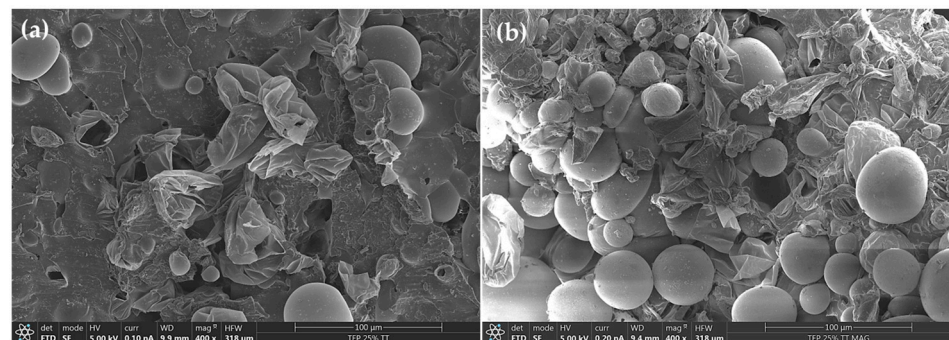


**Figure 10.** SEM micrographs obtained after debonding of the specimens (a) +25T and (b) +25MT.

#### 2.4. Durability

The durability test was performed using the wedge test according to ASTM D3762. Double cantilever beam specimens loaded by forcing a wedge between the beams. Crack growth over time is a commonly used test method to compare the durability of joints. The crack size length and fracture energy (Equation (6)) were evaluated at different times.  $E$  represents the aluminum Young's modulus (70.5 GPa),  $\Delta$  is the wedge thickness (3 mm),  $h$  corresponds to adherent thickness (6 mm), and crack length is denoted by  $a$ .

$$G_{Ic} = \frac{3 E h^3 \Delta^2}{16(a + 0.6h)^4} \quad (6)$$

Initial cracks measured 80.6 mm, 65.7 mm, and 55.4 mm for the pure resin, +25T, and +25MT, respectively (Figure 11a). The crack in the resin remained at this length until 168 h.

Subsequently, the crack length increased by 118.5 mm at 504 h, reaching 150 mm by 672 h, indicating continuous cracking until the end of the test.

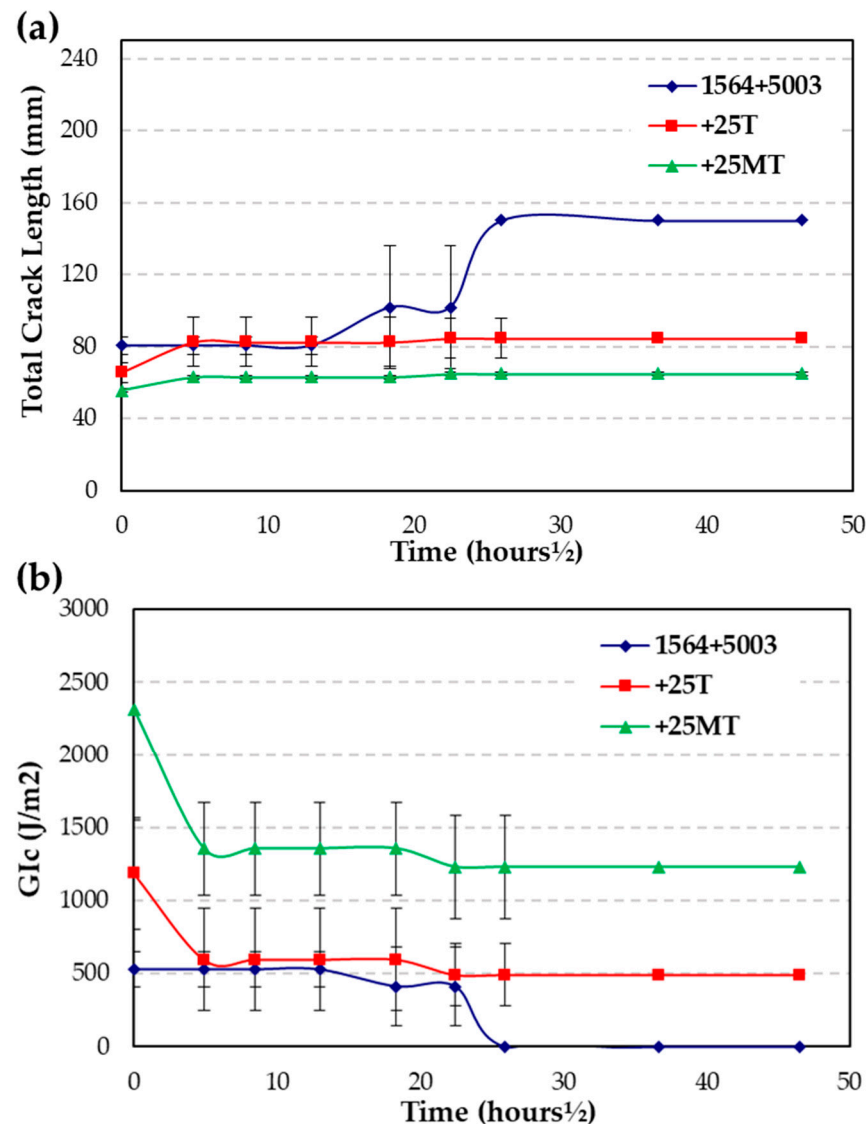


**Figure 11.** Wedge test durability parameters. (a) Crack length and (b) fracture energy.

As depicted in Figure 11a, the initial crack for the +25T adhesive measured 65.7 mm, expanding to 82.5 mm within the first 24 h. It remained at that length until 336 h when it increased to 84.6 mm, maintaining this length until the end of the 2160 h test. Similarly, for the +25MT adhesive, the crack growth was less than that of the +25T. Starting at 55.4 mm, it reached 63 mm at 24 h and extended to 64.9 mm by 336 h, persisting until the conclusion of the 2160 h test. This represents only 27% and 9% of the crack growth observed in the resin.

Regarding the fracture energy (Figure 11b), the energy diminished to zero as the specimen with pure resin fully opened. However, the filled adhesives maintained a constant fracture energy after 336 h, with higher energy observed for +25MT, which was attributed to the smaller crack growth.

### 2.5. Mobility of Particles within the Matrix and Recycling of Adherents

Figure 12a displays a sequence of frames captured from a video depicting the movement of magnetic TEP particles within epoxy resin. This movement is induced by running a magnet along the bottom of the container housing the particles. The arrangement of particles within an adhesive joint is achieved by employing magnets of various sizes and

adjusting the polarity of some relative to others [47], thereby directing the particles towards the center or edges depending on the desired adhesive modification.

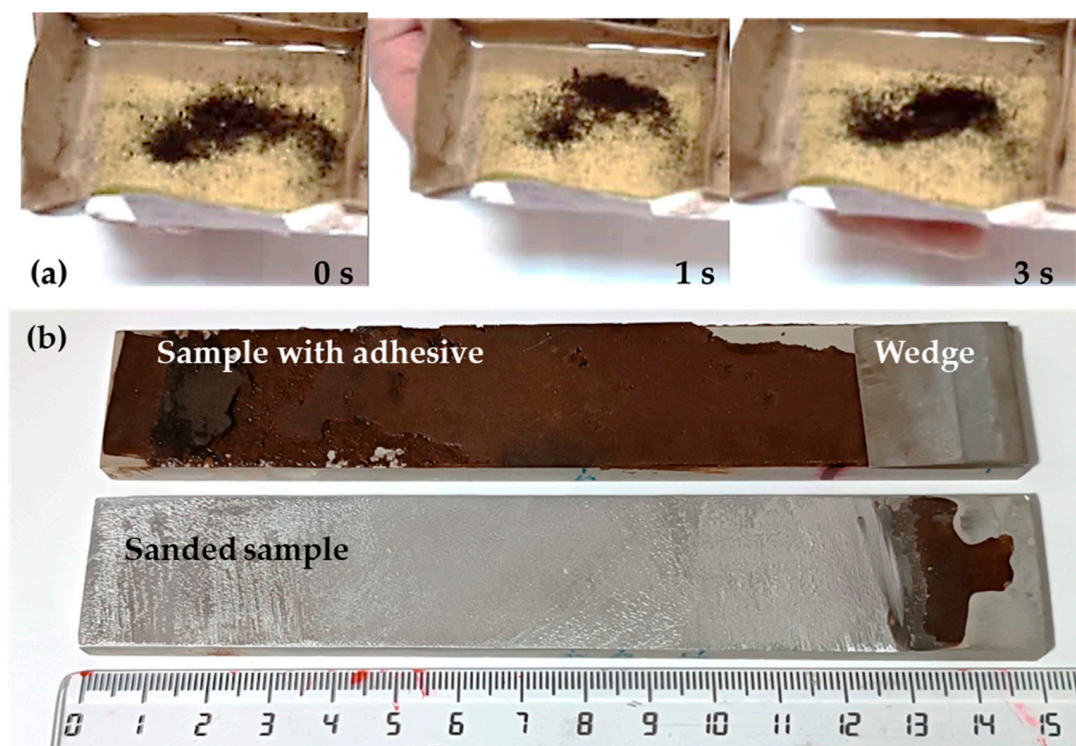


**Figure 12.** (a) Continuous frames of a video movie, and (b) recycling of a sample after heat breakage and sanding.

Figure 12b illustrates a sample subjected to aging in a wedge test followed by heating in an oven at 100 °C for 10 min to expand the TEPs. Upon separation of the adhesive bonding during the test, the wedge used for the experiment dislodged. Subsequently, one of the separated parts was sanded to assess the recyclability of the aluminum adherent. As depicted in Figure 12b, the sample was deemed ready to be reused.

### 3. Discussion

#### 3.1. Characterization of TEPs

TEPs are copolymers of ethylene and vinyl acetate [57], with their acetate content estimated at approximately 11%. Additionally, these types of polymers typically have aluminum and/or magnesium hydroxide fillers added to crosslink them, using silanes as crosslinking agents [58]. Their melting temperature is around 95 °C (Table 1, Figure 1).

During the treatments carried out, their properties and structure changed. Their crystallinity decreased during the plasma treatment by 9%, due to the kinetic energy input experienced by the molecules in a short time frame. During wet magnetization, the crystallinity decreased considerably by 50% (Figure 1, Table 1). This could be attributed to the strongly acidic and/or basic media used during the process or the subsequent freeze-drying process to remove excess water [55]. The crystallinity of the material cannot be calculated because the crystallinity of 100% crystalline TEPs is unknown. A peak corresponding to presence of water in magnetic TEPs was found, which was probably due to the magnetization process, where it became adsorbed on the surface, hence it evaporated at low temperatures.

NMR was used to observe the surface changes made with LPP treatment on TEPs (Figure 2). In this case, existing groups in the chain were also identified, although extrapolating to draw the polymer formula was not possible. The only change found was at 165

ppm, where a small doublet appeared, possibly due to the increase in or generation of ester groups in the chain, a group that typically appears in other polymers after plasma treatment, along with more oxygen-rich groups, such as carboxyls, hydroxyls, etc. [59].

SEM micrographs demonstrate that the TEPs particles have an average diameter of about 16  $\mu\text{m}$  (Figure 3a), and that LPP treatment does not destroy TEP microcapsules (Figure 3b). However, LPP gives the particles a different appearance due to a change in their surface roughness. In the case of magnetic TEPs, a crust deposited on the surface is visible; moreover, EDAX spectrum analysis performed on the SEM confirms the presence of Fe on the surface at around 23% and 1% of Mg, possibly added as a filler to the copolymer for crosslinking.

Characterization of the magnetic TEPs (Figure 4) using XRD clearly shows the peaks of magnetite ( $\text{Fe}_3\text{O}_4$ ) and compares them with the pattern of this oxide, allowing us to determine if any other iron oxide has formed on the surface, such as maghemite ( $\gamma\text{Fe}_2\text{O}_3$ ). However, the two oxides cannot be differentiated by X-rays as their patterns coincide. The planes found correspond to the cubic crystalline structure of the reverse spinel type, which is typical of magnetite.

### 3.2. Influence of the Addition of TEPs on Adhesive Curing Kinetics

The increase in the curing rate as temperature rose can be explained by the collision theory. According to this theory, particles can only react upon collision. As the temperature of a substance increases, its particles gain momentum, leading to a higher frequency of collisions. Thus, the reaction rate experiences acceleration (Figure 5) [60].

Epoxy resins cure through the presence of a hardener. This hardener serves to open the oxirane ring of the resin, thereby initiating the reaction. As a result, the oxirane ring generates OH groups that catalyze the reaction and facilitate crosslinking. The reaction concludes when there are no OH groups or hardener remaining to open additional oxirane rings. Consequently, there are two reaction mechanisms: an n-order mechanism at the outset and conclusion of the reaction, and an auto-catalytic mechanism occurring from 15–20% to 80% conversion.

Numerous empirical models have been developed to explore these effects in epoxy resins, given their applications as structural adhesives and in the production of composite materials, such as those incorporating carbon and glass fibers. Several models have been investigated in previous studies for both pure resins and composites [19,61,62]. In this work, Kamal's method has been chosen because it gives an idea of the two mechanisms, Equations (2) and (3) [63].

The curve fits provided by the Kamal equation differ (Figure 6). At a temperature of 40  $^\circ\text{C}$ , both auto-catalytic and n-order curing mechanisms take place. However, at higher temperatures, the heat input tends to favor the n-order mechanism due to the increased reaction speed caused by heightened collisions. This phenomenon occurs for both pure resin and composite materials, as the opening of the oxirane ring determines the occurrence of either mechanism.

Although the reaction mechanisms (auto-catalytic and n-order) typically remain consistent across composites and pure resin, particles within the composites may exert slight influence on these mechanisms. The presence of TEPs can inhibit the action of the hardener, since they contain OH groups that react with the amino groups. This would lead to less crosslinking, leaving uncured epoxy resin. In addition, TEPs can also cause steric hindrance and allow the chains to crosslink in the three-dimensional network [64]. Consequently, TEPs have the potential to accelerate or delay the reaction mechanisms.

The kinetic constants calculated from Equation (3) determine the controlling reaction at each temperature (Table 2). For pure resin, the auto-catalytic mechanism is slower at all temperatures, thus  $k_2$  determines the rate of curing. However, the composites show a lower  $k_1$ , so it is the n-order mechanism that controls the curing reaction. This aligns with the aforementioned explanation that the TEPs are deceiving the hardener and causing a delay in the opening of the oxirane ring.

In the n-order reaction, the energy required for the curing process is higher for +25T and +25 MT adhesives than for pure resin (Table 3). Therefore, the addition of particles requires more energy for the curing reaction. This is consistent with the steric hindrance caused by TEPs in the resin curing process and the reaction of the OH of the particles with the hardener amine. However, these effects do not impact the cross-linking of the adhesive, as the  $T_g$  does not decrease, although the viscosity increases, delaying the auto-catalytic reaction. Nevertheless, it is the n-order reaction that determines the curing rate.

### 3.3. Examine the Debonding Process Occurring Due to Temperature

In general, all three adhesives exhibit rigid behavior, though those containing TEPs (without and with magnetite) demonstrate a tougher disposition, with a shear modulus that is 15% lower. The 10% reduction in shear strength observed in the +25MT may result from the agglomerations of the magnetic particles, which attract one another. These agglomerations serve as stress accumulation points, contributing to the decrease in strength. However, TEPs are treated with plasma, thus ensuring a strong adhesion and effectively reinforcing the resin, thereby enhancing its strength for +25T.

The higher shear strength of the +25T adhesive, coupled with its elevated  $T_g$ , implies that it demands additional time and higher temperatures for debonding to take place. Consequently, there is a residual shear strength of 55% within the investigated time frames. However, the magnetic particles facilitate quicker and more efficient heat transmission, resulting in total debonding occurring at lower temperatures (10 min at 110 °C).

### 3.4. Durability

When the samples were subjected to 95% humidity and a temperature of 50 °C, the wedge test revealed the brittle nature of the pure resin, characterized by rapid crack propagation and a low fracture energy. In contrast, the filled adhesives exhibited an increased toughness, with a reduced crack growth that remained consistent from 336 h of testing to 2160 h. This higher resistance to environmental conditions may be due to stronger and higher adhesion and cohesion forces than pure resin.

The variances noted between the two filled adhesives may be due to the inherent characteristics of the TEPs. Prior to magnetization, the particles possess a soft nature, enabling deformation that facilitates crack advancement. Consequently, the crack may propagate more rapidly, resulting in a lower fracture energy. However, upon magnetization, the particle's crust hardens slightly, causing the crack to encircle it. This slows down crack propagation, leading to a higher fracture energy.

## 4. Materials and Methods

### 4.1. Materials

#### 4.1.1. Thermally Expandable Particles

Thermally expandable particles (TEPs), also known as microcapsules or microspheres, were pioneered by Dow Chemical Co in the early 1970s [65]. These particles consist of a thermo-plastic shell filled with liquid hydrocarbon. Upon heating, two transformations occur. Firstly, the shell material softens, and secondly, the hydrocarbon liquid inside undergoes gasification. Consequently, the shell expands as the gas pushes against it from the inside, causing it to increase in size. Upon full expansion, the particles volume can grow by a factor of 50 to 100 times. Upon cooling, the shell stiffens, and the particle remains in its expanded form. Expansion temperatures can vary from 70 °C to 285 °C depending on the particle type and grade [66].

LPP (Low Pressure Plasma) treatment is performed to modify and cleanse the surface of TEPs. This treatment increases surface energy and enhances their wettability, ensuring better adhesion with epoxy resin. Moreover, LPP treatment facilitates the adsorption of magnetite onto the surface of TEPs. Previous attempts without treatment demonstrated the challenges associated with adsorption on TEPs.

The LPP chamber plasma cleaner from Harrick Plasma (Ithaca, NY, USA) was utilized, employing air to generate plasma at a pressure of 40 Pa. The treatment duration lasted for 180 s under an electric power of 9 W. The process gas (air) was introduced into the chamber at flow rates typically ranging from 1 to 2 SCFH (standard cubic feet per hour) and at low to medium pressure (26–80 Pa). The chamber operates with an oscillating radio frequency (RF) electric field generated in the gas region through magnetic induction. The optimized operational parameters include the duration of time spent in the chamber and the power settings.

The magnetization process was carried out using the wet method following the cork magnetization patent [55].

#### 4.1.2. Epoxy Resin

The epoxy resin used was Araldite<sup>®</sup> LY 1564, supplied by Huntsman Advanced Materials (Everberg, Belgium), with hardener Aradur<sup>®</sup> 5003. The chemical composition of the epoxy resin includes 2,2'-(1-methylethylidene) bis(4,1-phenylenoxymethylene) bisoxirane (>70–<90% *w/w*), and 1,4-Bis(2,3-epoxypropoxy)butane (>10–<20% *w/w*). It is a clear liquid with a viscosity ranging between 0.2 and 1.4 Pa s and a density between 1.10 and 1.20 g cm<sup>-3</sup> at 25 °C. The hardener 5003 is solely composed of 3,6,9,12-Tetraazatetradecamethylenediamine. It appears as a clear light-yellow liquid with a viscosity ranging between 0.07 and 0.1 Pa s and a density between 0.98 and 1.08 g cm<sup>-3</sup> at 25 °C. The recommended epoxy to hardener ratio is 100:20 wt.

### 4.2. Characterization of Thermally Expandable Particles

#### 4.2.1. Differential Scanning Calorimetry

Differential scanning calorimetry (DSC) analysis was performed on untreated, treated, and magnetic TEPs. A DSC 822e supplied by Mettler Toledo GmbH (Greifensee, Switzerland) was used to examine the specimen's thermal properties. The scans were performed with a heating rate of 20 °C/min in a temperature range of –20 °C to 200 °C. Aluminum crucibles of 40 µL were used and filled with 1.5–3 mg of TEPs. The DSC tests were repeated three times for each condition and material to verify the repeatability of the results.

#### 4.2.2. Nuclear Magnetic Resonance

Solid state <sup>13</sup>C (100.73 MHz) CPMAS NMR spectra at 300 K employing a 4 mm DVT probe-head, were acquired using a Bruker WB 400 MHz spectrometer (NMR service, UNED-LAB, UNED) provided by Bruker España S.A. (Madrid, Spain). Samples were meticulously packed into 4 mm diameter cylindrical zirconia rotors with Kel-F end caps. The operational parameters included 3.2 µs 90° <sup>1</sup>H pulses and decoupling by spinal 64 sequence. Initially, the <sup>13</sup>C spectra were referenced to a glycine sample, and subsequently, the chemical shifts were recalibrated to Me<sub>4</sub>Si (δ (glycine) = 176.1 ppm for the carbonyl atom).

The typical acquisition parameters for <sup>13</sup>C CPMAS were as follows: spectral width, 40 kHz; recycle delay, 5 s; acquisition time, 30 ms; contact time, 2 ms; and spin rate, 12 kHz.

Only untreated and plasma treated TEPs can be analyzed with this technique.

#### 4.2.3. Scanning Electron Microscopy

Untreated, LPP-treated, and magnetic TEPs were analyzed using a Teneo SEM (ThermoFisher Scientific Inc., Waltham, MA, USA). The samples underwent preparation via gold coating in a Polaron high-resolution sputter coater (Quorum Technologies Ltd., Lewes, UK) to ensure a conductive medium for electrons, thereby producing sufficient contrast in the SEM micrographs. The energy of the electron beam was set at 2 kV. While EDAX (energy-dispersive X-ray) spectrum provides semiquantitative information, iron being a heavy element, the measurement error is lower compared to lighter elements.

#### 4.2.4. X-ray Diffraction

X-ray diffraction (XRD) analysis was conducted using a Philips PANalytical X'Pert Pro MRD system (Malvern PANalytical Limited, Malvern, UK). Intensity versus  $2\theta$  plots were acquired within an angular range spanning from  $10^\circ$  to  $90^\circ$ , with a step size of  $0.02^\circ$  and a step time of 2.4 s per step. The presence of magnetite was identified by the matching pattern number corresponding to magnetite (JCPDS No. 89-2355).

### 4.3. Characterization of Filled Adhesive

#### 4.3.1. Influence of TEPs on the Curing Kinetics of Epoxy Resin

Kinetic analysis offers crucial insights into the energy demand for driving the curing process and the underlying mechanisms. The inclusion of both varieties of TEPs can potentially alter these kinetic parameters, thereby influencing the thermal characteristics of the resin. Consequently, such modifications are not advisable.

DSC was also used to study the kinetic parameters. 40  $\mu\text{L}$  aluminum crucibles were employed, each containing approximately 8 mg of either the composite or pure resin for every test. Nitrogen served as the purge gas at a flow rate of 50 mL/min. Isothermal tests lasting 120 min were conducted at various temperatures (40, 60, and 80  $^\circ\text{C}$ ). Additionally, a secondary segment involved dynamic scanning from the isothermal temperature to 200  $^\circ\text{C}$  at a rate of 10  $^\circ\text{C}/\text{min}$  to calculate the total heat of reaction. Three trials were conducted for each condition.

#### 4.3.2. Influence of TEPs on the Debonding Process

The EN AW 6063-T6 aluminum alloy served as the substrate material for this investigation. Aluminum specimens underwent degreasing with a lanolin-free cloth soaked in methyl ethyl ketone (MEK), followed by shot-blasting with alumina, and a subsequent cleansing with MEK. Single-lap specimens were fabricated in accordance with the methodology outlined in standard EN 1465:2009 [67]. The aluminum specimens comprised two rectangular segments, each measuring 25 mm in width, 100 mm in length, and  $6 \pm 0.1$  mm in thickness. These segments were bonded together with an overlap length of 25 mm. Throughout the bonding process, the single-lap shear specimens were securely held in a fixture to ensure a consistent bond line. The average thickness of the bond line was  $0.8 \pm 0.1$  mm.

Following an 8 h period at room temperature, the adhesive bonds underwent post-curing at 60  $^\circ\text{C}$  for 4 h. Subsequently, the samples were left at room temperature to equilibrate. The shear strength of the specimens was assessed utilizing an Ibertest ELIB-20 tensile testing machine (manufactured by Ibertest, Madrid, Spain) equipped with a 20 kN load cell, operating at a crosshead speed of 1 mm/min.

Five replicates were tested for each experimental condition. The values presented in the graphs represent the average of five test specimens, with error bars indicating standard deviations.

Three adhesive joints were also fabricated to investigate debonding under identical conditions. Subsequently, they were placed into a Thermo-Fisher Scientific S.L. vacuum oven, Model VT6060 (Alcobendas, Madrid, Spain). The samples were introduced individually at 90  $^\circ\text{C}$ , and the temperature was incrementally raised until debonding occurred. Throughout the process, photographs were captured using a Canon digital camera Model PowerShot 595 (Canon España, S.A., Alcobendas, Madrid, Spain) and a FLIR infrared camera model E95 (FLIR Networked Systems S.L., Madrid, Spain).

#### 4.3.3. Influence of TEPs on Durability of Epoxy Resin

Wedge test samples were prepared with slight deviations from the EN 14444:2005 standard [68]. Aluminum EN AW 6063-T6, measuring 150 mm in length, 25 mm in width, and 6 mm in thickness, were utilized to prevent plastic deformation in the specimens. The adhesive was applied in a manner that left 19 mm bare at one end of the joint for wedge insertion. Teflon spacers were employed to regulate bond-line thickness, with an average

thickness of  $0.6 \pm 0.1$  mm. Following curing, wedges were fully inserted using a tensile testing machine at a constant rate of 10 mm/min.

Subsequent to wedge insertion, the specimens were stored for 24 h at room temperature in a desiccator before measuring the initial crack length. Both edges of each specimen were examined under a stereoscopic microscope (magnification  $\times 30$ ), and the crack tips were marked and measured. Subsequently, the specimens were subjected to  $95 \pm 2\%$  relative humidity at  $50^\circ\text{C}$  for 90 days (2160 h). The data presented in the graphs represent the average of three test specimens.

## 5. Conclusions

### 1. Main Novelty and Advantages:

- Debonding an adhesive bond manufactured with magnetic TEPs by heating offers significant advantages, reducing the energy required for the disassembly of adhesive bonds and facilitating the reuse of substrates, aligning with the principles of a circular economy.

### 2. Detailed Results:

- The TEPs' microcapsules open within a temperature range from  $90$  to  $130^\circ\text{C}$ , rendering thermal curing unfeasible at high temperatures.
- The curing process can be studied using Kamal's equation. The TEPs were found to influence the curing degree.
- The addition of TEPs or magnetic TEPs does not affect the melting temperature.
- The curing rate varies with temperature and the presence of TEPs.

### 3. General Results:

- TEPs significantly influence the curing process and mechanical properties of the adhesive.
- Magnetic TEPs can be manipulated with a magnet when they are embedded in the resin, allowing for a precise placement within the joint.
- The shear strength of adhesive bonds can be enhanced by the presence of TEPs, but magnetic TEPs reduce shear strength while increasing durability under the studied conditions of temperature and humidity.

### 4. Future Study Outlook:

- Further investigation is required to validate the performance of debonding technologies in practical applications.

**Author Contributions:** Conceptualization, J.A. and M.-A.M.; methodology, J.A. and J.-C.d.R.; software, J.A.; validation, J.A., M.-A.M. and J.-C.d.R.; formal analysis, J.A. and J.-C.d.R.; investigation, J.A. and J.-C.d.R.; resources, M.-A.M. and J.-C.d.R.; writing—original draft preparation, J.A.; writing—review and editing, S.L.d.A., M.-A.M. and J.-C.d.R.; visualization, J.A.; supervision, M.-A.M. All authors have read and agreed to the published version of the manuscript.

**Funding:** This research received no external funding.

**Data Availability Statement:** The data files from the equipment utilized, along with the Excel or Origin files used for calculations, are available upon specific request for any researchers or reviewers wishing to consult them.

**Acknowledgments:** We would like to thank the laboratory technicians of the Mechanical Engineering department of the ICAI, the laboratory of the Materials Science and Engineering department of the Carlos III University of Madrid, and the NMR Service—UNEDLAB for their technical support.

**Conflicts of Interest:** The authors declare no conflicts of interest.

## References

1. Sarfraz, M.S.; Hong, H.; Kim, S.S. Recent Developments in the Manufacturing Technologies of Composite Components and Their Cost-Effectiveness in the Automotive Industry: A Review Study. *Compos. Struct.* **2021**, *266*, 113864. [[CrossRef](#)]
2. Czerwinski, F. Current Trends in Automotive Lightweighting Strategies and Materials. *Materials* **2021**, *14*, 6631. [[CrossRef](#)] [[PubMed](#)]
3. Sakai, S.i.; Yoshida, H.; Hiratsuka, J.; Vandecasteele, C.; Kohlmeyer, R.; Rotter, V.S.; Passarini, F.; Santini, A.; Peeler, M.; Li, J.; et al. An International Comparative Study of End-of-Life Vehicle (ELV) Recycling Systems. *J. Mater. Cycles Waste Manag.* **2014**, *16*, 1–20. [[CrossRef](#)]
4. D'Adamo, I.; Gastaldi, M.; Rosa, P. Recycling of End-of-Life Vehicles: Assessing Trends and Performances in Europe. *Technol. Forecast. Soc. Chang.* **2020**, *152*, 119887. [[CrossRef](#)]
5. Jang, Y.C.; Choi, K.; Jeong, J.; Kim, H.; Kim, J.-G. Recycling and Material-Flow Analysis of End-of-Life Vehicles towards Resource Circulation in South Korea. *Sustainability* **2022**, *14*, 1270. [[CrossRef](#)]
6. Mura, M.; Longo, M.; Zanni, S. Circular Economy in Italian SMEs: A Multi-Method Study. *J. Clean. Prod.* **2020**, *245*, 118821. [[CrossRef](#)]
7. Li, Y.; Fujikawa, K.; Wang, J.; Li, X.; Ju, Y.; Chen, C. The Potential and Trend of End-of-Life Passenger Vehicles Recycling in China. *Sustainability* **2020**, *12*, 1455. [[CrossRef](#)]
8. Shah, V.; Bhaliya, J.; Patel, G.M.; Deshmukh, K. Advances in Polymeric Nanocomposites for Automotive Applications: A Review. *Polym. Adv. Technol.* **2022**, *33*, 3023–3048. [[CrossRef](#)]
9. Agarwal, J.; Sahoo, S.; Mohanty, S.; Nayak, S.K. Progress of Novel Techniques for Lightweight Automobile Applications through Innovative Eco-Friendly Composite Materials: A Review. *J. Thermoplast. Compos. Mater.* **2020**, *33*, 978–1013. [[CrossRef](#)]
10. Kawajiri, K.; Kobayashi, M.; Sakamoto, K. Lightweight Materials Equal Lightweight Greenhouse Gas Emissions?: A Historical Analysis of Greenhouse Gases of Vehicle Material Substitution. *J. Clean. Prod.* **2020**, *253*, 119805. [[CrossRef](#)]
11. Cavezza, F.; Boehm, M.; Terryn, H.; Hauffman, T. A Review on Adhesively Bonded Aluminium Joints in the Automotive Industry. *Metals* **2020**, *10*, 730. [[CrossRef](#)]
12. Perez, M.; Akhavan-Safar, A.; Carbas, R.J.C.; Marques, E.A.S.; Wenig, S.; da Silva, L.F.M. Loading Rate and Temperature Interaction Effects on the Mode I Fracture Response of a Ductile Polyurethane Adhesive Used in the Automotive Industry. *Materials* **2022**, *15*, 8948. [[CrossRef](#)] [[PubMed](#)]
13. Bruckner, T.M.; Singewald, T.D.; Gruber, R.; Hader-Kregl, L.; Müller, M.; Kern, C.; Hafner, M.; Paulik, C. Influence of Hollow Glass Microspheres on 1K Epoxy Structural Adhesive for the Automotive Industry. *Int. J. Adhes. Adhes.* **2023**, *124*, 103396. [[CrossRef](#)]
14. Rosendo, D.; Viana, G.; Carbas, R.; Marques, E.; da Silva, L.F. Effect of Temperature and Moisture on the Impact Behaviour of Adhesive Joints for the Automotive Industry. *J. Appl. Comput. Mech.* **2021**, *7*, 1488–1500. [[CrossRef](#)]
15. Marques, A.C.; Mocanu, A.; Tomić, N.Z.; Balos, S.; Stammen, E.; Lundevall, A.; Abrahami, S.T.; Günther, R.; de Kok, J.M.M.; de Freitas, S.T. Review on Adhesives and Surface Treatments for Structural Applications: Recent Developments on Sustainability and Implementation for Metal and Composite Substrates. *Materials* **2020**, *13*, 5590. [[CrossRef](#)] [[PubMed](#)]
16. Galvez, P.; Abenojar, J.; Martinez, M.A. Effect of Moisture and Temperature on the Thermal and Mechanical Properties of a Ductile Epoxy Adhesive for Use in Steel Structures Reinforced with CFRP. *Compos. Part B Eng.* **2019**, *176*, 107194. [[CrossRef](#)]
17. Encinas, N.; Lavat-Gil, M.; Dillingham, R.G.; Abenojar, J.; Martínez, M.A. Cold Plasma Effect on Short Glass Fibre Reinforced Composites Adhesion Properties. *Int. J. Adhes. Adhes.* **2014**, *48*, 85–91. [[CrossRef](#)]
18. Abenojar, J.; Tutor, J.; Ballesteros, Y.; del Real, J.C.; Martínez, M.A. Erosion-Wear, Mechanical and Thermal Properties of Silica Filled Epoxy Nanocomposites. *Compos. Part B Eng.* **2017**, *120*, 42–53. [[CrossRef](#)]
19. Abenojar, J.; Lopez de Armentia, S.; Barbosa, A.Q.; Martinez, M.A.; del Real, J.C.; da Silva, L.F.M.; Velasco, F. Magnetic Cork Particles as Reinforcement in an Epoxy Resin: Effect of Size and Amount on Thermal Properties. *J. Therm. Anal. Calorim.* **2023**, *148*, 1981–1995. [[CrossRef](#)]
20. Shishesaz, M.; Hosseini, M. Effects of Joint Geometry and Material on Stress Distribution, Strength and Failure of Bonded Composite Joints: An Overview. *J. Adhes.* **2020**, *96*, 1053–1121. [[CrossRef](#)]
21. Adams, R.D.; Cooper, D.G.A.; Pearson, S. Vibration Damping of Adhesively Bonded Joints. In *Handbook of Adhesion Technology*; da Silva, L.F., Öchsner, A., Adams, R.D., Eds.; Springer International Publishing: Cham, Switzerland, 2021; pp. 854–875, ISBN 978-3-319-55410-5.
22. Koh, E.; Park, S. Self-Anticorrosion Performance Efficiency of Renewable Dimer-Acid-Based Polyol Microcapsules Containing Corrosion Inhibitors with Two Triazole Groups. *Prog. Org. Coat.* **2017**, *109*, 61–69. [[CrossRef](#)]
23. Madhi, A. Smart Epoxy/Polyurethane/Carbon Quantum Dots Hybrid Coatings: Synthesis and Study of UV-Shielding, Viscoelastic, and Anti-Corrosive Properties. *Polym. Plast. Technol. Mater.* **2023**, *62*, 403–418. [[CrossRef](#)]
24. Baena, M.D. Debonding of Structural Adhesive Joints. In *Structural Adhesive Joints: Design, Analysis and Testing*; Mittal, K.L., Panigrahi, S.K., Eds.; John Wiley & Sons, Inc.: Hoboken, NJ, USA, 2020; pp. 135–138. ISBN 978111973643.
25. Kemal, A. Functionally Graded Adhesively Bonded Joints. In *Progress in Adhesion and Adhesives*; Mittal, K.L., Ed.; John Wiley & Sons, Inc.: Hoboken, NJ, USA, 2015; pp. 57–78. ISBN 9781119162193.
26. Das, R.-R. Failure Analysis of Structural Adhesive Joints with Functionally Graded Tubular Adherends. In *Structural Adhesive Joints: Design, Analysis and Testing*; Mittal, K.L., Panigrahi, S.K., Eds.; John Wiley & Sons, Inc.: New York, NY, USA, 2020; pp. 205–219. ISBN 9781119736431.

27. dos Reis, M.Q.; Marques, E.A.S.; Carbas, R.J.C.; da Silva, L.F.M. Functionally Graded Adherends in Adhesive Joints: An Overview. *J. Adv. Join. Process.* **2020**, *2*, 100033. [[CrossRef](#)]
28. Li, R.; Noda, N.A.; Takaki, R.; Sano, Y.; Takase, Y.; Miyazaki, T. Most Suitable Evaluation Method for Adhesive Strength to Minimize Bend Effect in Lap Joints in Terms of the Intensity of Singular Stress Field. *Int. J. Adhes. Adhes.* **2018**, *86*, 45–58. [[CrossRef](#)]
29. Goodenough, J.; Fitzgerald, A.; Bean, K.; Hatcliffe, J.; Slark, A.; Hamerton, I.; Bond, I. Reversible Adhesives and Debondable Joints for Fibre-Reinforced Plastics: Characteristics, Capabilities, and Opportunities. *Mater. Chem. Phys.* **2023**, *299*, 127464. [[CrossRef](#)]
30. Budhe, S.; Banea, M.D.; de Barros, S.; da Silva, L.F.M. An Updated Review of Adhesively Bonded Joints in Composite Materials. *Int. J. Adhes. Adhes.* **2017**, *72*, 30–42. [[CrossRef](#)]
31. Tenorio-Alfonso, A.; Sánchez, M.C.; Franco, J.M. A Review of the Sustainable Approaches in the Production of Bio-Based Polyurethanes and Their Applications in the Adhesive Field. *J. Polym. Environ.* **2020**, *28*, 749–774. [[CrossRef](#)]
32. Gonçalves, F.A.M.M.; Santos, M.; Cernadas, T.; Ferreira, P.; Alves, P. Advances in the Development of Biobased Epoxy Resins: Insight into More Sustainable Materials and Future Applications. *Int. Mater. Rev.* **2022**, *67*, 119–149. [[CrossRef](#)]
33. Roig, A.; Ramis, X.; De la Flor, S.; Serra, À. Eugenol-Based Dual-Cured Materials with Multiple Dynamic Exchangeable Bonds. *Eur. Polym. J.* **2024**, *206*, 112782. [[CrossRef](#)]
34. Carbonell-Blasco, M.P.; Moyano, M.A.; Hernández-Fernández, C.; Sierra-Molero, F.J.; Pastor, I.M.; Alonso, D.A.; Arán-Aís, F.; Orgilés-Calpena, E. Polyurethane Adhesives with Chemically Debondable Properties via Diels–Alder Bonds. *Polymers* **2024**, *16*, 21. [[CrossRef](#)]
35. Roig, A.; Molina, L.; Serra, À.; Santiago, D.; De la Flor, S. Structural Reversible Adhesives Based on Thiol-Epoxy Vitrimers. *Polym. Test.* **2023**, *128*, 108205. [[CrossRef](#)]
36. Avshalomov, R.; Jarach, N.; Dodiuk, H. Breaking the Unbreakable Bond: Towards Sustainable Adhesives' Future. *Eur. Polym. J.* **2024**, *209*, 112920. [[CrossRef](#)]
37. Banea, M.D.; Da Silva, L.F.M.; Campilho, R.D.S.G.; Sato, C. Smart Adhesive Joints: An Overview of Recent Developments. *J. Adhes.* **2014**, *90*, 16–40. [[CrossRef](#)]
38. Banea, M.D.; Da Silva, L.F.M.; Carbas, R.J.C.; Campilho, R.D.S.G. Structural Adhesives Modified with Thermally Expandable Particles. *J. Adhes.* **2015**, *91*, 823–840. [[CrossRef](#)]
39. Banea, M.D.; Da Silva, L.F.M.; Carbas, R.J.C.; Campilho, R.D.S.G. Mechanical and Thermal Characterization of a Structural Polyurethane Adhesive Modified with Thermally Expandable Particles. *Int. J. Adhes. Adhes.* **2014**, *54*, 191–199. [[CrossRef](#)]
40. Banea, M.D.; Da Silva, L.F.M.; Carbas, R.J.C. Debonding on Command of Adhesive Joints for the Automotive Industry. *Int. J. Adhes. Adhes.* **2015**, *59*, 14–20. [[CrossRef](#)]
41. Banea, M.D.; da Silva, L.F.M.; Carbas, R.J.C.; de Barros, S. Debonding on Command of Multi-Material Adhesive Joints. *J. Adhes.* **2017**, *93*, 756–770. [[CrossRef](#)]
42. Banea, M.D.; Da Silva, L.F.M.; Carbas, R.; Barros, S.D.E. Effect of Temperature and Moisture on the Tensile Properties of a TEPS-Modified Adhesive. *Mater. Plast.* **2018**, *55*, 478–481. [[CrossRef](#)]
43. Banea, M.D.; Da Silva, L.F.M.; Carbas, R.J.C.; Cavalcanti, D.K.K.; De Souza, L.F.G. The Effect of Environment and Fatigue Loading on the Behaviour of TEPS-Modified Adhesives. *J. Adhes.* **2020**, *96*, 423–436. [[CrossRef](#)]
44. Piazza, G.; Burczyk, M.; Gerini-Romagnoli, M.; Belingardi, G.; Nassar, S.A. Effect of Thermally Expandable Particle Additives on the Mechanical and Reversibility Performance of Adhesive Joints. *J. Adv. Join. Process.* **2022**, *5*, 100088. [[CrossRef](#)]
45. Banea, M.D.; da Silva, L.F.M.; Carbas, R.J.C.; Barbosa, A.Q.; de Barros, S.; Viana, G. Effect of Water on the Behaviour of Adhesives Modified with Thermally Expandable Particles. *Int. J. Adhes. Adhes.* **2018**, *84*, 250–256. [[CrossRef](#)]
46. Ciardiello, R.; Martorana, B.; Lambertini, V.G.; Brunella, V. Iron-Based Reversible Adhesives: Effect of Particles Size on Mechanical Properties. *Proc. Inst. Mech. Eng. Part C J. Mech. Eng. Sci.* **2018**, *232*, 1446–1455. [[CrossRef](#)]
47. da Silva, C.I.; Barbosa, A.Q.; Marques, J.B.; Carbas, R.C.; Marques, E.A.S.; Abenojar, J.; da Silva, L.F. Mechanical Characterisation of Graded Single Lap Joints Using Magnetised Cork Microparticles. In *Advanced Joining Processes in Advanced Structured Materials*; Öchsner, A., da Silva, L.F., Altenbach, H., Eds.; Springer: Singapore, 2019; Volume 125, pp. 153–174, ISBN 978-981-15-2956-6.
48. da Silva, C.I.; Cunha, M.R.O.; Barbosa, A.Q.; Carbas, R.J.C.; Marques, E.A.S.; da Silva, L.F.M. Functionally Graded Adhesive Joints Using Magnetic Microparticles with a Polyurethane Adhesive. *J. Adv. Join. Process.* **2021**, *3*, 100048. [[CrossRef](#)]
49. Carbas, R.J.C.; Da Silva, L.F.M.; Critchlow, G.W. Adhesively Bonded Functionally Graded Joints by Induction Heating. *Int. J. Adhes. Adhes.* **2014**, *48*, 110–118. [[CrossRef](#)]
50. Saeedifar, M.; Saleh, M.N.; De Freitas, S.T.; Zarouchas, D. Damage Characterization of Adhesively-Bonded Bi-Material Joints Using Acoustic Emission. *Compos. Part B Eng.* **2019**, *176*, 107356. [[CrossRef](#)]
51. Özer, H.; Öz, Ö. The Use of the Exponential Drucker-Prager Material Model for Defining the Failure Loads of the Mono and Bi-Adhesive Joints. *Int. J. Adhes. Adhes.* **2017**, *76*, 17–29. [[CrossRef](#)]
52. Chiminelli, A.; Breto, R.; Izquierdo, S.; Bergamasco, L.; Duvivier, E.; Lizaranzu, M. Analysis of Mixed Adhesive Joints Considering the Compaction Process. *Int. J. Adhes. Adhes.* **2017**, *76*, 3–10. [[CrossRef](#)]
53. Bonaldo, J.; Banea, M.D.; Carbas, R.J.C.; Da Silva, L.F.M.; De Barros, S. Functionally Graded Adhesive Joints by Using Thermally Expandable Particles. *J. Adhes.* **2019**, *95*, 995–1014. [[CrossRef](#)]
54. Carbas, R.J.C.; da Silva, L.F.M.; Andrés, L.F.S. Functionally Graded Adhesive Joints by Graded Mixing of Nanoparticles. *Int. J. Adhes. Adhes.* **2017**, *76*, 30–37. [[CrossRef](#)]

55. Abenojar, J.; López de Armentia, S.; Barbosa, A.Q.; Martínez, M.A.; Velasco, F.; da Silva, L.F.M.; del Real Romero, J.C. Coating Cork Particles with Iron Oxide: Effect on Magnetic Properties. *Wood Sci. Technol.* **2020**, *54*, 869–889. [[CrossRef](#)]
56. Mohammadkhani, F.; Montazer, M.; Latifi, M. Microwave Absorption Characterization and Wettability of Magnetic Nano Iron Oxide/Recycled PET Nanofibers Web. *J. Text. Inst.* **2019**, *110*, 989–999. [[CrossRef](#)]
57. Wang, K.; Deng, Q. The Thermal and Mechanical Properties of Microinhomogeneous Materials. *Polymers* **2019**, *11*, 1055. [[CrossRef](#)]
58. Cárdenas, M.A.; García-López, D.; Gobernado-Mitre, I.; Merino, J.C.; Pastor, J.M.; de Martínez, J.D.; Barbeta, J.; Calveras, D. Mechanical and Fire Retardant Properties of EVA/Clay/ATH Nanocomposites—Effect of Particle Size and Surface Treatment of ATH Filler. *Polym. Degrad. Stab.* **2008**, *93*, 2032–2037. [[CrossRef](#)]
59. Abenojar, J.; Martínez, M.A.; Velasco, F.; Rodríguez-Pérez, M.A. Atmospheric Plasma Torch Treatment of Polyethylene/Boron Composites: Effect on Thermal Stability. *Surf. Coat. Technol.* **2014**, *239*, 70–77. [[CrossRef](#)]
60. Moore, J.W.; Pearson, R.G. *Kinetics and Mechanism*, 3rd ed.; John Wiley & Sons, Inc.: New York, NY, USA, 1981; ISBN 0-471-03558-0.
61. Abenojar, J.; Enciso, B.; Pantoja, M.; Velasco, F.; Martínez, M.A. Thermal Characterization and Diffusivity of Two Mono-Component Epoxies for Transformer Insulation. *Int. J. Adhes. Adhes.* **2020**, *103*, 102726. [[CrossRef](#)]
62. Abenojar, J.; de Armentia, S.L.; Martínez, M.A.; del Real, J.C. Development of a Green Epoxy Adhesive for Cork by Adding Lignin: Thermal and Bonding Properties. *Wood Sci. Technol.* **2022**, *56*, 721–742. [[CrossRef](#)]
63. Kamal, M.R.; Sourour, S. Kinetic and Thermal Characterization of Thermoset Cure. *Polym. Eng. Sci.* **1973**, *13*, 59–64. [[CrossRef](#)]
64. Paz-Abuin, S.; Pazos-Pellin, M.; Paz-Paxos, M. Influence of the Reactive of Amine Hydrogens and the Evaporation of Monomers on the Cure Kinetics of Epoxy-Amine: Kinetic Questions. *Polymer* **1997**, *38*, 3795–3804. [[CrossRef](#)]
65. Morehouse, D.S.; Tetreault, R.J. Expandable Thermoplastic Polymer Particles Containing Volatile Fluid Foaming Agent and Method of Foaming the Same 1967. U.S. Patent No. 3,615,972, 26 October 1971.
66. Thermo-Expandable Microcapsule. Matsumoto Microsphere®F and FN Series. Available online: <https://www.mtmtys.co.jp/e/product/general/data01.html> (accessed on 11 December 2023).
67. EN 1465:2009; Adhesives—Determination of Tensile lap-Shear Strength of Bonded Assemblies. JIS: Tai Po Kau, Hong Kong, 2008.
68. EN 14444:2005/AC:2008; Structural Adhesives—Qualitative Assessment of Durability of Bonded Assemblies—Wedge Rupture Test. ISO: Geneva, Switzerland, 2008.

**Disclaimer/Publisher’s Note:** The statements, opinions and data contained in all publications are solely those of the individual author(s) and contributor(s) and not of MDPI and/or the editor(s). MDPI and/or the editor(s) disclaim responsibility for any injury to people or property resulting from any ideas, methods, instructions or products referred to in the content.